INVESTIGATING THE LIMITS OF ENCELADUS'S TIDALLY DRIVEN TIGER STRIPE FAILURE SCENARIO: EXPLORATION OF ICE SHELL THICKNESS, COEFFICIENT OF FRICTION, AND FAULT DEPTH.

John Olgin[1], Bridget R. Smith-Konter[1], and Robert T. Pappalardo[2]. [1] University of Texas at El Paso, 500 West Univeristy Avenue, El Paso, TX 79968 (jolgin@miners.utep.edu, brkonter@utep.edu). [2]Jet Propulsion Laboratory, California Institute of Technology, M/S 183-301, Pasadena, CA 91109 (Robert.pappalardo@jpl.nasa.gov).

Introduction: Cassini observations of the south polar region of Enceladus revealed four large linear fractures associated with anomalous temperature gradients and active plumes [1, 2]. These features, referred to as "tiger stripes," are now thought to be the source of tectonic strike-slip and/or oblique open-close motions [3,4,5], similar to those of the faulting regimes inferred for Jupiter's moon Europa [6]. These motions are likely a result of tidally induced stresses that are exerted on a satellite during its daily orbital (diurnal) cycle around its parent body.

In this study, we investigate tidally driven stresses of Enceladus's tiger stripes and their resulting Coulomb failure potential over a complete Enceladus tidal cycle. While previous studies have followed a similar approach to investigate individual modes of failure (shear vs. normal) of the tiger stripes [3, 4], this work differs in that: (1) contributions of both shear and normal stress are considered [5], and (2) we investigate the role of ice shell thickness, coefficient of friction, and fault depth (Figure 1). In particular, the thickness of Enceladus's ice shell and the depth of its underlying ocean plays an important role in determining the magnitude and orientation of the tidal stresses on the surface of the satellite [6,7]. Combining these ideas, we pose the question: *What is the upper bound on the thickness of Enceladus's ice shell and the range of frictional coefficients and fault depths that support Coulomb failure activity along the tiger stripe fault segments?*

Here we present preliminary results demonstrating tidal effects on the Coulomb failure criterion as a function of ice shell thickness. As an example, we demonstrate Coulomb failure behavior of the tiger stripes for ice shell thicknesses ranging from 6-40 km for the first half of Enceladus's orbit (Figure 2). Overall, we find that the spatial and temporal window for Coulomb failure, i.e. for potential fault activity, decreases across the entire tiger stripe fault system with increasing ice thickness. In particular, we find that ice shell thicknesses greater than 40 km do not support the conditions necessary for fault failure on Enceladus. Future applications of this approach are valid for deformation studies of Europa and other icy moons of the outer solar system where diurnal stress variations are important.

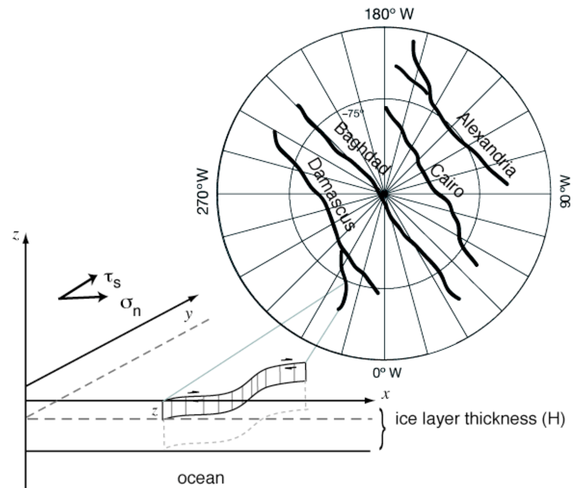

Figure 1. Polar stereographic projection of Enceladus's tiger stripes and 3D sketch of faults, extended to a depth *z*, embedded in icy outer shell. Shear and normal stress magnitudes and orientation depend on the assumed Love numbers applicable for each ice shell model and the geometry of each fault segment. Coulomb stresses ultimately depend on these stresses, an assumed coefficient of friction, and the overburden depth at which the stresses are analyzed.

Tidal Stress Modeling: We assume that diurnal tidal stresses provide sufficient driving forces for shear and normal fault motions to occur along the tiger stripe fractures. To extract the tidal diurnal stress components, we utilize the program SatStress [7], a numerical modeling code that calculates the 2D tidal stress tensor at any point on the surface of an icy satellite for diurnal and/or non-synchronous rotation stresses. We adopt the following common parameters for models demonstrated here: shear modulus $\mu = 3.5$ GPa, Poisson ratio $\nu = 0.33$, gravity $g = 0.11$ m/s^2, ice density $\rho = 0.92$ g/cm^3, radius $r = 252$ km, satellite mass = 1.08×10^{20} kg, orbital semi-major axis = 238 $\times 10^3$ km, and eccentricity $e = 0.0047$. We assume a constant upper rigid ice layer thickness $H_u = 3$ km and viscosity $\eta_u = 10^{22}$ Pa s, and lower ice layer viscosity $\eta_l = 10^{13}$ Pa s [3]. To test the sensitivity of stresses to variable total ice shell thicknesses, we calculate Love numbers appropriate for Enceladean ice shells of thickness H = 6, 24, 30, 40, 50, 75 and 90 km, underlain by a global subsurface ocean that extends to a total ice shell + ocean depth of 95 km. These Love numbers range from h_2 = 0.25 – 0.02 and l_2 = 0.068 – 0.002, with Love numbers decreasing in magnitude with increasing ice shell thickness.

Using these parameters, we calculate tidal diurnal stresses in the region of the tiger stripe fractures for each ice shell model. We resolve shear (τ_s) and normal (σ_n) stresses onto discrete tiger stripe fault elements of specified orientation [3,5,8]. Shear stresses approach peak amplitudes of ~81 kPa, 63 kPa, 55 kPa, 41 kPa, 29 kPa, 11kPa and 6 kPa for H = 6, 24, 30, 40, 50, 75 and 90 km models, respectively, throughout the tidal cycle.

To investigate the failure conditions along each fault segment as a function of orbital position, we use a modified version of the Coulomb failure criterion ($\sigma_f = \tau_s - \mu_f(\sigma_n + \rho gz)$), which depends on the shear and normal stresses, the overburden pressure (ρgz), and the effective coefficient of friction (μ_f). According to this model, frictional sliding will occur on optimally oriented fault segments when the resolved shear stress exceeds the frictional resistance on the fault. In the example model discussed here (Figure 2), we assume a constant fault depth z = 2 km and μ_f = 0.2 [5]. We compute Coulomb stress for each ice shell thickness model to identify regions of the fault system that are more or less likely to fail throughout the tidal cycle for a given set of applied conditions.

Preliminary Results: Using the Coulomb failure criterion, it is feasible to predict failure direction, frequency, and location along each tiger stripe throughout the orbital cycle. Figure 2 demonstrates the variable Coulomb stresses generated by models of varying ice shell thickness (6 km, 24 km, 30 km, and 40 km). During one complete orbital cycle, models with ice thicknesses between 6 km and 30 km show a steady decline in fault activity, while models with ice thicknesses > 40 km show a fault failure scenario that is completely inactive.

Based on these preliminary models, at periapse (m = 0°), Enceladus experiences regions of both locked and slipping fault motions for the 6 and 24 km models, and virtually no slipping regions for the 30 and 40 km models. As Enceladus advances in orbital position, positive Coulomb stresses begin to dominate the 6 km model, showing a very active slip scenario, while variable locked and slipping conditions are present for the 24 and 30 km models. The 40 km model appears locked throughout the entire orbit.

We are presently compiling a suite of frictional coefficient and fault depth dependent models to investigate the limits of Coulomb failure of the tiger stripe fault system. Previous work [5], assuming a 24 km ice shell thickness, limited fault failure to models with μ_f = 0.1 - 0.3 and fault depths = 2 – 4 km. Tectonic activity inferred from this analysis positively correlates with temperature anomalies at the tiger stripes, however, in detail some regions of the model do not strongly match the observations. The preliminary results discussed here and laboratory-derived ice fracture experiments will provide the basis for a more in-depth parameter search. Future work will focus on tuning the model to allow for variable fault segment frictional and fault geometry parameters, to best simulate the available plume and temperature anomaly data.

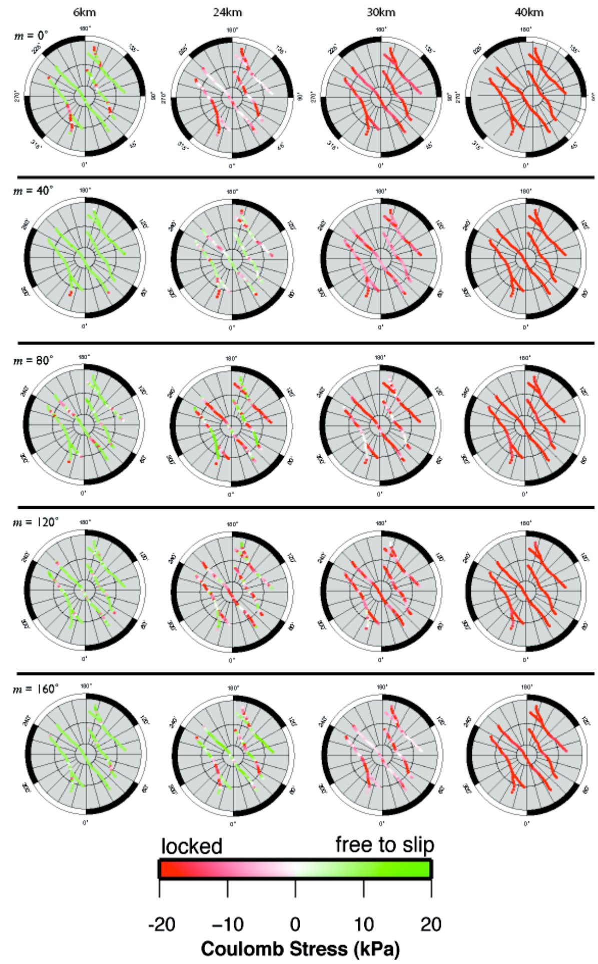

Figure 2. Coulomb stresses for a 6, 24, 30, and 40 km thick ice shell model (left to right), captured at 40° orbital increments from periapse (0°) through periapse + 160°. Negative Coulomb stresses (red) imply a locked fault, while positive stresses (green) imply conditions supporting fault slip.

References:. [1] Porco, C.C. et al. (2006), *Science*, 311, 1393-1401. [2] Spencer, J.R. et al. (2006), *Science*, 311, 1401-1405. [3] Nimmo, F. et al. (2007), *Nature*, 447, 289-291. [4] Hurford, T.A. et al. (2007), *Nature*, 447, 292-294. [5] Smith-Konter, B., and R.T. Pappalardo (2008), *Icarus,* 198, 435 – 451. [6] Hoppa, G.V. et al. (1999), *Icarus,* 141, 287-298. [7] Wahr, J. et al. (2008), *Icarus*, 200, 188-206. [8] King.G.C.P. et al. (1994) *BSSA*, 84, 935-953. [9] Olgin, J.G. et al. (2009) *GSA*, Abstract # 166275.